Human-Inspired Control of Dual-Arm Exoskeleton Robots With Force and Impedance Adaptation

Zhijun Li, *Senior Member, IEEE*, Cuichao Xu, Qiang Wei, Chao Shi, and Chun-Yi Su, *Senior Member, IEEE*

***Abstract*—Humans can adapt to complex environments by voluntarily adjusting the impedance parameters and interaction force. Traditional robots perform tasks independently without considering their interactions with the external environment, which leads to poor flexibility and adaptability. Comparatively, humans can adapt to complex environments by voluntarily adjusting the impedance parameters and interaction force. In order to solve the problems of human–robot security and adaptability to unknown environment, a human-inspired control with force and impedance adaptation is proposed to interact with unknown environments and exhibit this biological behavior on the developed dual-arm exoskeleton robots. First, we propose a computationally model utilizing the sampled surface electromyogram (sEMG) signals to calculate the human arm endpoint stiffness and define a co-contraction index to describe the dynamic behaviors of the muscular activities in the tasks. Then, the obtained human limb impedance stiffness parameters and the sampling position information are transferred to the slave arm of the exoskeleton as the input variables of the controller in real-time. In addition, a variable stiffness observer is used here to compensate for the errors of the calculated stiffness by sEMG signals. The experimental studies of human impedance transfer control have been conducted to show the effectiveness of the developed approach. Results of the experimental suggest that the proposed controller can achieve human motor adaptation and enable the subjects to execute a skill transfer control by a dual-arm exoskeleton robot.**

***Index Terms*—Impedance control, adaptive robust control, human-robot interaction, robotic exoskeleton, stiffness identification.**

Manuscript received August 1, 2018; accepted September 11, 2018. This work was supported in part by the National Natural Science Foundation of China under Grant 61573147, Grant 61625303, and Grant 61751310, in part by the National Key Research and Development Program of China under Grant 2017YFB1302302, in part by the Guangdong Science and Technology Research Collaborative Innovation Projects under Grant 2014B090901056, Grant 2015B020214003, and Grant 2016A020220003, in part by the Guangdong Science and Technology Plan Project (Application Technology Research Foundation) under Grant 2015B020233006, and in part by the Anhui Science and Technology Major Program under Grant 17030901029. This paper was recommended by Associate Editor S. Nahavandi. *(Corresponding author: Zhijun Li.)*

Z. Li, C. Xu, and Q. Wei are with the Department of Automation, University of Science and Technology of China, Hefei 230026, China (e-mail: zjli@ieee.org).

C. Shi was with the College of Automation Science and Engineering, South China University of Technology, Guangzhou 510006, China. He is now with China Merchants Bank Network Technology in Shenzhen, Guangdong, China.

C.-Y. Su is with the School of Automation, Guangdong University of Technology, Guangzhou 510006, China, on leave from the Department of Mechanical Engineering, Concordia University, Montreal, QC H3G 1M8, Canada (e-mail: cysu@alcor.concordia.ca).

Color versions of one or more of the figures in this paper are available online at http://ieeexplore.ieee.org.

Digital Object Identifier 10.1109/TSMC.2018.2871196

I. Introduction

INSPIRED by the human dual arm structure, dual-arm exoskeleton can perform as a human power augment device, in rehabilitation training, etc., or straightforwardly enhance the capability of humans in daily tasks [1], [2], [26]–[30]. Dual-arm exoskeletons can provide motion support to humans, especially to the elder or the patients with impaired muscles that are not able to generate necessary amount of forces to perform intended tasks. Besides, dual-arm exoskeleton can be used in some dual-arm coordination tasks. For example, patients can use the dual-arm exoskeleton and adjust the behavior of the healthy side to the affected side so as to achieve the purpose of rehabilitation training. Thus, exhibiting biological behavior and performance of the developed exoskeletons is necessary. However, the dual-arm exoskeleton brings various human–robot interaction problems in the manipulation and makes the coordination of two arms greatly difficult as well. Therefore, it is necessary to investigate the control strategy accordingly to the task requirements and handle the human–robot interaction problems at the same time. Recently, teleoperation technologies have attracted a considerable amount of interest around the world due to their widespread applications, such as in remote handling hazardous materials, underwater maintenance, robotic telesurgery, and repairing tasks [31]. In [35], some challenging issues in bilateral teleoperation control design was taken into consideration, such as the communication delay, various nonlinearities, parameter variations, and modeling uncertainties existing in manipulator and environment dynamics. To deal with these control issues, a globally stable nonlinear adaptive robust control algorithm was developed for bilateral teleoperation systems. In an attempt to overcome the limitations of conventional teleoperation interfaces, the concept of tele-impedance control had been presented in [4], and there are several related interaction tasks presented to verify the effectiveness of the control concepts [5], [6]. In this paper, EMG signals is used for controlling the tele-impedance system in the real-time because of the advantages of easy accessibility, fast adaptivity, and stability.

It has been verified that the impedance of the human arm can be voluntarily adapted during motion [7], [25]. According to [8], to realize a strict impedance control, one need to get the interaction forces (using force sensor) and a fixed model of the impedance is required as well. However, considering the situation where the environment is uncertain, keeping the interaction stable becomes difficult, if we ignore the interaction forces, the impedance control would lost its accuracy. There

are some works presented to optimize the impedance control and propose the variable impedance actuators (VIAs) [9]. Imitating the behavior of human, VIA can adapt the stiffness with only a little energy consumption, which is able to match the intrinsic safety, energy efficiency, and motion performance of biological systems. However, concretizing these potentialities requires some special algorithms to adapt force and impedance to the task and the dynamic environment.

Considering that human limb interacts with the unknown environment, the human would adjust his limb adaptively with the changed interaction force, when there are no interactions, muscles would be back to be relaxing state. Neuromotor experimental studies have shown that the impedance of human joints can be voluntarily adapted during motion tasks and we want to use this human-like adaptation skills on the robot so that the robot can solve the complexity and redundancy in an elegant, effective, and coordinated manner and it would also greatly benefit the physical human–robot interaction. To solve the problems of human–robot security and adaptability to unknown environment, and exhibit the biological behavior (adjusting impedance parameters) on the developed dual-arm exoskeleton robots considering poor flexibility and adaptability of traditional robots, we need to design the control that uses the surface electromyography (sEMG) signals to obtain stiffness and position of the human left arm (master) in real-time and then transfer the profiles to the right arm of the exoskeleton (slave) as the reference command, adapting the stiffness accordingly to the interaction force or the dynamic environment.

A lot of research results show that the surface electromyography signals have close relationships with the muscle activations, muscular force, and limb configuration. Therefore, sEMG signals are widely used in the stiffness modulation mechanisms to obtain the endpoint stiffness. In [10], the task is only about the fixed posture configuration, a simple model assuming that a linear relationship between end-point stiffness and processed sEMG signals was used. However, the linear model does not describe the estimation of the workspace stiffness unless a complex modeling of the musculo-skeletal system was provided [11]. Related researches on human motor behavior presented that the complexity can be solved by the central nervous system in an efficient way [12], [13].

In order to compensate for the instability of the control system caused by uncertain dynamics, some adaptive control methods can be applied. For instance, in [32], an adaptive control with neural networks was proposed to estimate the unknown dynamics caused by friction and comparative experimental results revealed the improved performance. In [33], an alternative continuous robust adaptive control method was presented for servo mechanisms, and the unknown nonlinear dynamics are approximated by using an echo state networks. Extensive experimental results showed the continuous robust control can lead to smoother control response and reduced oscillations in the control responses. In [34], three adaptive parameter estimation algorithms were discussed and then used to estimate the parameters of nonlinear robotic systems. By simulation, the theoretical analysis was confirmed. After the external disturbance and system uncertainty are parameterized, the adaptive control law will track the predetermined trajectory accurately. However, when the nonparametric uncertainty is encountered in the adaptive process, the adaptive law may not perform well. In this paper, a human-inspired control framework for dual-arm exoskeleton robot with force and impedance adaptation has been established. Ajoudani *et al.* [15] explored how the arm geometry and muscular contraction influenced the endpoint stiffness, and proved that the master is able to adjust the size of the stiffness by changing the co-activation of the arm muscles, while changing the endpoint stiffness direction through adjusting the arm posture. In this paper, we shall exploit the sEMG signals to acquire the stiffness of the human arm and transfer it to the exoskeleton arm provided as the input command for the designed control. In addition, we have compensated for the errors of the calculated stiffness by using a variable stiffness observer. To verify the effectiveness of the proposed method, we have conducted a specific experiment on the developed dual-arm exoskeleton robot. The experimental results show that the proposed control method can achieve human motor adaptation through transferring the stiffness from the human arm to the slave robot arm, and fulfill the skill transfer control task using the developed dual-arm exoskeleton robot.

To summarize, in this paper, a human-inspired control framework for dual-arm exoskeleton robot with force and impedance adaptation has been established to exhibit the human-like behavior. We shall exploit the sEMG signals to acquire the stiffness of the human arm and transfer it to the exoskeleton arm provided as the robot input command for the designed control. In addition, to make a good performance we have compensated for the errors of the calculated stiffness by using a variable stiffness observer. To verify the effectiveness of the proposed method, we have conducted a specific experiment on the developed dual-arm exoskeleton robot. The experimental results show that the proposed control method can achieve human motor adaptation through transferring the stiffness from the human arm to the slave robot arm, and fulfill the skill transfer control task using the developed dual-arm exoskeleton robot. The contributions of this paper are listed as follows.

1) A human-inspired controller for a dual-arm exoskeleton robot is proposed based on human skills transfer, where the human impedance parameters and position profiles are transferred to the slave robot arm.
2) The impedance parameters stiffness is computed from the sEMG signals collected from human muscles in real-time.
3) An adaptive-robust impedance controller considering unknown dynamics is developed to drive the slave arm of exoskeleton tracking the desired trajectories and is able to make the tracking errors convergence when the perturbations exist.

II. Cartesian Stiffness Modeling of Human Arm

A. Conservative Stiffness Matrix

Consider the different dimension between joint space and Cartesian space, the congruence transformation with the

Fig. 1. Dual-arm exoskeleton robot.

stiffness matrices in two spaces can be described as a nonconservative mapping [17], one can use the transformation

$$K_J(q) = J_r^T(q) K_s(q) J_r(q) \tag{1}$$

where $K_J(q) \in \mathbb{R}^{n\times n}$, n is the joint space dimension, $K_J(q)$ denotes the joint stiffness matrices and $K_s(q) \in \mathbb{R}^{m\times m}$, m denotes the task space dimension, $K_s(q)$ denotes the end-point stiffness matrices, both of them are related to the joint angle vector q, since the dimensions between the two space are usually unequal, the Jacobian matrix $J_r(q) \in \mathbb{R}^{m\times n}$ of the manipulator is assumed to be nonsingular in the finite work space Ω. If two spaces have the equal dimension, one can has that m is actually equal to n. In this paper, we assume $m = n$. According to [18], the inverse transform can be described as

$$K_s(q) = \left(J_r^{-1}(q)\right)^T K_J(q) (J_r(q))^{-1} \tag{2}$$

where $J_r^{-1}(q)$ denotes the inverse matrix of $J_r(q)$. From the theory of the kinematics of robots, Jacobian matrix is totally dependent on the configuration of the robot, in other words, the matrix J_r would change as q of the robot in real time, which shows that the stiffness matrix is configuration-dependent and changing over time.

B. Cartesian Stiffness Modeling of Human Arm

It has been proven that through adjusting the mechanical properties of the upper limbs, human is capable of adapting the perturbation in the unknown environment [7]. However, in the human–robot interaction task, applying the adaptation skills to robot control by the human operator has turned out to be a challenge [16]. In general, there are three components (posture of arm, muscle co-contraction activity, stretch reflexes) contributing our human arm stiffness [19], which shows that we can acquire the desired end-point stiffness of the human upper limb through contracting of relevant muscle groups or adjusting the pose of the arm's configuration. Ajoudani *et al.* [15] have shown that it is reasonable to neglect the effect caused by the pose configuration on the joint stiffness matrix in some specific cases. Then, the joint stiffness $K_J \in \mathbb{R}^{n\times n}$ can be represented as

$$K_J = a_{cc} \bar{K}_J \tag{3}$$

where $\bar{K}_J$ denotes the intrinsic constant matrix at minimum muscle activity, a_{cc} indicates the co-contraction index, which is estimated by the muscular activation level according to [6] and [37]

$$a_{cc} = 1 + \frac{r_1\left[1 - e^{-r_2(P_B+P_T)}\right]}{\left[1 + e^{-r_2(P_B+P_T)}\right]} \tag{4}$$

where P_B and P_T denote the sEMG signals of the dominant antagonistic muscle pairs, r_1 and r_2 are two unknown parameters to be identified in the experiment. Then, according to [15], we can obtain the end-point stiffness of the human limb K_s as

$$K_s(q) = \left(J_r^{-1}(q)\right)^T \left[K_J - \frac{\partial \tau_g(q)}{\partial q}\right] (J_r(q))^{-1} \tag{5}$$

where $K_s \in \mathbb{R}^{m\times m}$ denotes the end point stiffness, $q \in \mathbb{R}^n$ is a vector of n joint rotation angles, $J_r(q)$ denotes the human arm Jacobian matrix, and $\tau_g(q)$ denotes the gravitational torque vector. According to [15], $\tau_g(q)$ can be estimated in a compact model by

$$\tau_g(q) = \sum_{i=1}^{n_J} J_{com_i}^T(q) g m_i \tag{6}$$

where J_{com_i} indicates the center of mass Jacobian, m_i denotes the mass of the ith limb, n_J is the numbers of robot joint, while g is the gravitational accelerations vector.

III. Human Arm Endpoint Stiffness Estimation

From the description of (3) and (5), we need to obtain $a_{cc}, \bar{K}_J, J_r(q), \tau_g(q)$. First, the items $\tau_g(q)$ and the Jacobian matrix $J_r(q)$ can be easily obtained since all the parameters are measurable or computable values. Then, we obtain the two items a_{cc} and $\bar{K}_J$. According to [20], the active joint stiffness is highly related to muscular activations, and one can estimate that muscular activations by using sEMG signals.

Since the end-point stiffness matrix K_s is used for the dynamics cases, thus, it has to been identified in different configurations and different co-contraction amplitude of human arm. During the experiment, we sampled three different co-contraction levels of the human arm muscle groups and the minimum-activity trials is selected to estimate $\bar{K}_J$, others are employed for the identification of index a_{cc}.

We have chosen four different positions of the arm pose configuration in the whole experiments, while all the configurations satisfy two conditions: 1) the operator is comfort and 2) avoiding the Jacobian matrix to be singularity. In each experiment, arm joints were allowed to vary within the redundant manifold of the corresponding configuration to realize three distinct angles of the related joint. It gives rise to 12 arm configurations altogether. Furthermore, in each configuration, the operator was asked to select three different co-contraction levels of the arm muscle: 1) the minimum muscular activity; 2) the middle muscular activity; and 3) the high muscular activity. Finally, we can have 36 group data in the estimation of the end-point stiffness.

Since the sEMG signal is a weak electrical signal, the range of useful signal frequency is approximately from 0 to 500 in the published literature. Therefore, after the initial

signals were sampled, a band-pass filter (10–500HZ) and a notch filter (50HZ) were used to acquire the relatively pure signal (Butterworth filtering was chosen in the experiment). According to [15] and [21], multiple-input and multiple-output dynamics of the endpoint impedance can be decomposed into the linear subsystems associating each input to output. Thus, the dynamic relation between the displacements of the arm endpoint and endpoint force can be expressed as

$$\begin{bmatrix} F_x(f) \\ F_y(f) \end{bmatrix} = \begin{bmatrix} N_{xx}(f) & N_{xy}(f) \\ N_{yx}(f) & N_{yy}(f) \end{bmatrix} \begin{bmatrix} x(f) \\ y(f) \end{bmatrix} \tag{7}$$

where $F_x(f)$ and $F_y(f)$ are the Fourier transforms of the endpoint forces, $x(f)$ and $y(f)$ are the transforms of the human endpoint displacements. To identify the transfer function of each subsystems in (7), a nonparametric algorithm combined with the windowing techniques in frequency domain using MATLAB was adopted. Consequently, N_{ij} denotes the parametric second-order linear model of each impedance transfer function presented as

$$N_{ij}(s) = I_{sij}s^2 + V_{sij}s + K_{sij}, \quad s = 2\pi f\sqrt{-1} \tag{8}$$

where I_s denotes the endpoint inertia, V_s denotes the endpoint viscosity, and K_{sij} denotes the element in row i, column j in the matrix K_s.

Therefore, we can estimate human arm endpoint intrinsic constant stiffness $\bar{K}_s$ according to (7) and (8). Then, we can obtain the intrinsic joint stiffness matrix $\bar{K}_J$ by minimizing the following expression using the minimum activity groups:

$$\left\| \bar{K}_J - J_r^T(q)\bar{K}_s J_r(q) - \frac{\partial \tau_g(q)}{\partial q} \right\|. \tag{9}$$

Finally, the middle and the high muscular activity trials are used to obtain the two parameters r_1 and r_2 in (4) by minimizing

$$\left\| a_{cc}(p)\bar{K}_J - J_r^T(q)\bar{K}_s J_r(q) - \frac{\partial \tau_g(q)}{\partial q} \right\|. \tag{10}$$

In short, the transformation between the joint stiffness and the Cartesian stiffness can be modeled by (5). To identify $\bar{K}_J$ and a_{cc}, first, we estimated the Cartesian stiffness $\bar{K}_s$ offline using stochastic perturbation method in three different co-contraction levels of arm muscles. Then by minimizing (9), the intrinsic joint stiffness $\bar{K}_J$ can be obtained in the minimum co-contraction levels of arm muscles, and by minimizing (10) in other two co-contraction levels of arm muscles, the constants r_1, r_2 can be identified. Finally, the co-contraction index a_{cc} can be obtained by the sEMG signals in real time by (4), joint stiffness can be calculate by the model (3), and the endpoint stiffness K_s can be obtained by the transformation between the joint stiffness and the Cartesian stiffness modeled by (5). The above steps have been described more clearly in Table I.

The steps of EMG-based stiffness estimation are summarized in Table I.

TABLE I
STEP OF STIFFNESS IDENTIFICATION

Process: The Step of Stiffness Identification
1. Obtain arm endpoint stiffness ($\bar{K}_s$) offline in three different co-contraction levels (minimum, mid, high) of arm muscles based on stochasic perturbations method.
2. Identify the joint intrinstic constant stiffness ($\bar{K}_J$) by minimizing Eq. (9) with the group of minimum co-contraction levels and identify the coefficient ($a_{cc}(p)$) with other two group of co-contraction levels by minimizing Eq. (10), and obtain r_1 and r_2 according to Eq. (4).
3. Calculate the joint stiffness (K_J) by Eq. (3) with real-time sEMG signals and obtain the real-time endpoint stiffness K_s by the transformation between the joint stiffness and the Cartesian stiffness modelled by Eq. (5).

IV. CONTROL DEVELOPMENT OF SLAVE EXOSKELETON

The model of a n-link robotic exoskeleton can be expressed as follows:

$$M(q)\ddot{q} + C(q,\dot{q})\dot{q} + G(q) = \tau + \tau_{\text{int}} \tag{11}$$

where $q = [q_1, q_2, \ \ldots, \ q_n]^T \in R^n$ denotes the joint angles vector, $M(q) \in R^{n\times n}$ denotes the inertia matrix which should be symmetric positive and definite, while $C(\dot{q}, q) \in R^{n\times n}$ represents the matrix of Centripetal and Coriolis torques, $G(q) \in R^n$ represents the gravitational torque vector, $\tau \in R^n$ is a torque vector and $\tau_{\text{int}} \in R^n$ is an interaction torque vector.

Considering the Cartesian task space, we can define $x = [x_1, x_2, \ \ldots, \ x_n]^T \in R^n$ as the Cartesian position, and the relationship between $x \in R^n$ and $q \in R^n$ can be described as

$$\dot{x} = J_r\dot{q} \tag{12}$$

where $J_r \in R^{n\times n}$ denotes Jacobian matrix. We take the derivative of (12) on its both sides respect to time, and have the following:

$$\ddot{x} = J_r\ddot{q} + \dot{J}_r\dot{q}. \tag{13}$$

Assuming the Jacobian matrix J_r is nonsingular, we have

$$\ddot{q} = J_r^{-1}\left(\ddot{x} - \dot{J}_r\dot{q}\right). \tag{14}$$

Defining the end-point position errors as $e = x - x_d$, $\dot{e} = \dot{x} - \dot{x}_d$, $\ddot{e} = \ddot{x} - \ddot{x}_d$, where $x_d = [x_{d1}, x_{d2}, \ldots, x_{dn}]^T \in R^n$ is the reference position. We consider a damper-spring model as $f = M\ddot{e} + D\dot{e} + K_s e$, where $f = [f_1, f_2, \ldots, f_n]^T$ is the applied force, $M = \text{diag}[M_1, M_2, \ldots, M_n]$ is the inertia matrix, $D = \text{diag}[D_1, D_2, \ldots, D_n]$ is the damper matrix, $K_s = \text{diag}[K_{s1}, K_{s2}, \ldots, K_{sn}]$ is the stiffness matrix. Consider an additional unknown force function $g_i(e_i, u_i(t))$ [24], then we have

$$f_i = M_i\ddot{e}_i + D_i\dot{e}_i + K_{si}e_i + g_i(e_i, u_i(t)) \tag{15}$$

where $i = 1, 2, \ldots, n$, $u_i(t)$ is the stiffness-regulating input and bounded with its first derivative $\dot{u}_i(t)$. K_{si} means the vector in row i in the matrix K_s. Let $(\partial g_i(e_i, u_i(t))/\partial e_i) = K_{ei}(e_i, u_i(t))$ denote the stiffness to be measured. We define $\hat{K}_{ei}$ as the estimate of K_{ei} at time t, and $\tilde{K}_{ei} = K_{ei} - \hat{K}_{ei}$ is the stiffness estimation error. Differentiating (15) with respect to time, we can obtain

$$\dot{f}_i = M_i\dddot{e}_i + D_i\ddot{e}_i + K_{si}\dot{e}_i + K_{ei}\dot{e}_i + g_{ui}\dot{u}_i \tag{16}$$

where $g_{ui} = (\partial g_i(e_i, u_i(t))/\partial u_i)$. The estimate of $\dot{\hat{f}}_i$ [ignoring the item $g_{ui}(e_i, u_i)$ and $u_i(t)$] can be expressed as

$$\dot{\hat{f}}_i = M_i\dddot{e}_i + D_i\ddot{e}_i + K_{si}\dot{e}_i + \hat{K}_{ei}\dot{e}_i \tag{17}$$

where $\hat{K}_{ei}$ is the estimate of stiffness and considering the following update law:

$$\dot{\hat{K}}_{ei} = \varsigma_i \dot{\tilde{f}}_i \mathrm{sgn}(\dot{e}_i) \tag{18}$$

with $\dot{\tilde{f}}_i = \dot{f}_i - \dot{\hat{f}}_i$, $\varsigma_i > 0$ is selected by the designer and

$$\mathrm{sgn}(\bullet) = \begin{cases} \frac{\bullet}{\|\bullet\|}, & \|\bullet\| \neq 0 \\ 0, & \|\bullet\| = 0. \end{cases}$$

Remark 1: The existence of sign-function in (18) may inevitably lead to chattering in control torques. To avoid chattering, a sat-function can be used to replace the sign function [36].

Considering the Lyapunov candidate function with $\tilde{K}_{ei} = K_{ei} - \hat{K}_{ei}$

$$V_k = \sum_{i=1}^{n} \frac{1}{2} \tilde{K}_{ei}^2. \tag{19}$$

V_k is a Lyapunov function of stiffness estimation errors which is a part of (27) to verify the convergence of stiffness estimation error. One can obtain its derivative as

$$\begin{aligned} \dot{V}_k &= \sum_{i=1}^{n} \tilde{K}_{ei} \dot{\tilde{K}}_{ei} \\ &= \sum_{i=1}^{n} \left(\tilde{K}_{ei} \dot{K}_{ei} - \varsigma_i \tilde{K}_{ei} g_{ui} \dot{u}_i \mathrm{sgn}(\dot{e}_i) - \varsigma_i \tilde{K}_{ei}^2 |\dot{e}_i| \right) \\ &\leq \sum_{i=1}^{n} \left(\tilde{K}_{ei} \dot{K}_{ei} - \varsigma_i \tilde{K}_{ei} g_{ui} \dot{u}_i \mathrm{sgn}(\dot{e}_i) \right) \end{aligned} \tag{20}$$

when $|\tilde{K}_{ei}| > |g_{ui}|(|\dot{u}_i|/\dot{e}_i) + (1/\varsigma_i)(\dot{K}_{ei}/\dot{e}_i)$ holds, one can get that $\dot{V}_k \leq 0$. Thus, $\hat{K}_{ei}$ is turned out to uniformly convergence to the true stiffness value K_{ei}.

The manipulator impedance control model in Cartesian space was given by $M\ddot{e} + D\dot{e} + Ke = \mathcal{U}_r$, where $M \in R^{n\times n}$, $D \in R^{n\times n}$, $K \in R^{n\times n}$ denote the desired inertia, the desired damping and the desired stiffness matrices, respectively, $\mathcal{U}_r \in R^n$ can be regarded as the interaction force. From [38] and [39], the human limb model is largely related to the damper and spring items, it is reasonable to neglect the inertia term in (21), then the target impedance model can be written as

$$D\dot{e} + Ke = \mathcal{U}_r. \tag{21}$$

According to [40], since D and K are unknown, it is difficult to calculate x_d even if we can obtain the accurate force $\mathcal{U}_r$ by force sensor. In [23], two experiments had proved that the desired impedance of a system can be calculated from EMG signals. In this paper, we shall consider the calculated stiffness $K_s \in R^{n\times n}$ by the sampling sEMG signals of the human forearm to calculate the stiffness K_s, and from [22], there is the experimental data suggested that the relationships between joint stiffness and the damping can be expressed as

$$D = \varrho \sqrt{K_s} \tag{22}$$

where ϱ is used to adjust the damping of the system.

Considering that the stiffness calculated by sEMG signals may be not accurate enough, the variable stiffness observer (18) is utilized to compensate for the errors of the stiffness calculated by sEMG signals. The update law of the compensation item of the stiffness is given by

$$\dot{\hat{K}}_{ei} = \varsigma_i \dot{\hat{\mathcal{U}}}_{ri} sgn(\dot{e}_i) \tag{23}$$

where $\dot{\tilde{\mathcal{U}}}_{ri} = \dot{\mathcal{U}}_{ri} - \dot{\hat{\mathcal{U}}}_{ri}$ and $\hat{\mathcal{U}}_{ri} = D_i \dot{e}_i + K_{si} e_i + \hat{K}_{ei} e_i$. K_s stands for the stiffness calculated by sEMG signals and $\hat{K}_e$ stands for the compensation item of stiffness by stiffness observer. Although stiffness transferred by the human can be used as control signals for the robot manipulation, it may be not accurate enough due to unknown force. We utilize the stiffness observer to make a good performance on disturbance rejections and to achieve small tracking errors. Meanwhile, we have proved that $\tilde{K}_e$ is convergent so $\hat{K}_e$ is approximate to K_e. Thus, we have $K = K_s + \hat{K}_e$.

From the principal of virtual work, the end-point torque can be transferred into joint space as

$$\tau_{\mathrm{int}} = J_r^T \mathcal{U}_r \tag{24}$$

where τ_{int} denotes the interaction torque in joint space. Integrating (12), (14) into (11), we can obtain

$$\mathcal{M}\ddot{x} + \mathcal{C}\dot{x} + \mathcal{G} = \mathcal{U} + \mathcal{U}_r \tag{25}$$

where

$$\begin{aligned} \mathcal{M} &= J_r^{-T} M(q) J_r^{-1} \\ \mathcal{C} &= J_r^{-T}(-M(q)J_r^{-1}\dot{J}_r + C(q,\dot{q}))J_r^{-1} \\ \mathcal{G} &= J_r^{-T} G(q) \\ \mathcal{U} &= J_r^{-T}\tau. \end{aligned}$$

In the following, we will give some properties of the dynamic (25), which should be useful at later when we design the control system.

Property 1: The matrix $\dot{\mathcal{M}} - 2\mathcal{C}$ is skew-symmetric which maintains $\forall u \in R^n$, $u^T(\dot{\mathcal{M}} - 2\mathcal{C})u \equiv 0$.

Property 2: There exist be some finite positive constants $c_k > 0$ $(1 \leq k \leq 3)$ to keep inequalities $\forall x \in R^n$, $\forall \dot{x} \in R^n$, $||\mathcal{M}|| \leq c_1$, $||\mathcal{C}|| \leq c_2$, and $||\mathcal{G}|| \leq c_3$ are established, and one can get a vector $C = [c_1, c_2, c_3]^T$.

Defining $e = x - x_d$, $\dot{x}_r = \dot{x}_d - \lambda e$, $s = \dot{e} + \lambda e$, where λ is a positive definite diagonal matrix, while the designed control law is

$$\begin{aligned} \mathcal{U} &= -K_m s - \sum_{i=1}^{3} \frac{s\hat{c}_i \Phi_i^2}{\|s\|\Phi_i + \delta_i} - D\dot{e} - Ke \\ \dot{\hat{c}}_i &= -\sigma_i \hat{c}_i + \frac{\gamma_i \Phi_i^2 \|s\|^2}{\Phi_i \|s\| + \delta_i} \end{aligned} \tag{26}$$

where $K_m \in R^{n\times n}$ is a positive definite matrix, $\Phi = [\Phi_1, \Phi_2, \Phi_3]^T = [\|\ddot{x}_r\|, \|\dot{x}_r\|, 1]^T$; while $\gamma_i > 0$, $\delta_i(t) > 0$, and $\sigma_i(t) > 0$ such that $\int_0^t \delta_i(\omega)d\omega = a_i < \infty$ and $\int_0^t \sigma_i(\omega)d\omega = b_i < \infty$, in the actual implementation, we choose $\delta_i = 15/(1+t)^2$, $\sigma_i = 15/(1+t)^2$ in the experiment.

Consider the Lyapunov candidate function with $\tilde{c}_i = \hat{c}_i - c_i$ and remove $\sum_{i=1}^{n}(1/2)\tilde{K}_{ei}^2$ for simplicity

$$V_1 = \frac{1}{2} s^T \mathcal{M} s + \sum_{i=1}^{3} \frac{1}{2\gamma_i} \tilde{c}_i^2 + \sum_{i=1}^{n} \frac{1}{2} \tilde{K}_{ei}^2. \tag{27}$$

Noting that $\dot{\mathcal{M}} - 2\mathcal{C}$ is skew-symmetric, using (20), (25) and (26), we can obtain

$$\begin{aligned}
\dot{V}_1 &= s^T(\mathcal{M}\dot{s} + \mathcal{C}s) + \sum_{i=1}^{3}\frac{\tilde{c}_i\dot{\tilde{c}}_i}{\gamma_i} + \sum_{i=1}^{n}\tilde{K}_{ei}\dot{\tilde{K}}_{ei} \\
&\le s^T(\mathcal{M}(\ddot{x} - \ddot{x}_r) + \mathcal{C}(\dot{x} - \dot{x}_r)) + \sum_{i=1}^{3}\frac{\tilde{c}_i\dot{\tilde{c}}_i}{\gamma_i} \\
&= s^T(\mathcal{U} + \mathcal{U}_r - \mathcal{G} - \mathcal{M}\ddot{x}_r - \mathcal{C}\dot{x}_r) + \sum_{i=1}^{3}\frac{\tilde{c}_i\dot{\tilde{c}}_i}{\gamma_i} \\
&= s^T\Bigg(-K_m s - \sum_{i=1}^{3}\frac{s\hat{c}_i\Phi_i^2}{\|s\|\Phi_i + \delta_i} - D\dot{e} - Ke \\
&\qquad + \mathcal{U}_r - \mathcal{G} - \mathcal{M}\ddot{x}_r - \mathcal{C}\dot{x}_r\Bigg) + \sum_{i=1}^{3}\frac{\tilde{c}_i\dot{\tilde{c}}_i}{\gamma_i} \\
&\le -s^T K_m s - \sum_{i=1}^{3}\frac{\|s\|^2\hat{c}_i\Phi_i^2}{\|s\|\Phi_i + \delta_i} + \sum_{i=1}^{3}\frac{\tilde{c}_i\dot{\tilde{c}}_i}{\gamma_i} + \sum_{i=1}^{3}\|s\|c_i\Phi_i \\
&= -s^T K_m s + \sum_{i=1}^{3}\frac{\Phi_i\|s\|c_i\delta_i}{\Phi_i\|s\| + \delta_i} - \sum_{i=1}^{3}\frac{\sigma_i}{\gamma_i}(c_i + \tilde{c}_i)\tilde{c}_i \\
&\le -s^T K_m s - \sum_{i=1}^{3}\frac{\sigma_i}{2\gamma_i}\tilde{c}_i^2 + \sum_{i=1}^{3}\frac{\Phi_i\|s\|c_i\delta_i}{\Phi_i\|s\| + \delta_i} + \sum_{i=1}^{3}\frac{\sigma_i}{2\gamma_i}c_i^2 \\
&\le \varpi V_1 + \Lambda \qquad (28)
\end{aligned}$$

where $\varpi = \min((\lambda_{\min}(K_m)/\lambda_{\max}(\mathcal{M})), \min_{i=1,2,3}(\sigma_i))$ and $\Lambda = \sum_{i=1}^{3}[\Phi_i\|s\|c_i\delta_i/(\Phi_i\|s\| + \delta_i)] + \sum_{i=1}^{3}(\sigma_i/2\gamma_i)c_i^2$, $\varpi \ge 0$, for $\mathcal{M}$ and K_m are positive matrix and $\sigma_i(t) > 0$. Integrating the above inequation, we can obtain

$$V_1(t) \le \left(V_1(0) - \frac{\Lambda}{\varpi}\right)e^{-\varpi t} + \frac{\Lambda}{\varpi} \le V_1(0) + \frac{\Lambda}{\varpi}. \qquad (29)$$

Hence, for s, we can obtain $(1/2)s^T\mathcal{M}s \le V_1(0) + (\Lambda/\varpi)$, then $\|s\| \le [(2(V_1(0) + (\Lambda/\varpi)))/\lambda_{\min}(\mathcal{M})]$, similarly, $\|\tilde{c}_i\| \le 2(V_1(0) + (\Lambda/\varpi))\max_{i=1,2,3}(\gamma_i)$. Thus, the error signals s and $\tilde{c}_i$ are bounded, and $s \to 0$ and $\tilde{c}_i \to 0$ as $t \to \infty$ with the convergence rate $e^{-\varpi t}$. Consequently, $e \to 0$, $\dot{e} \to 0$ as $t \to \infty$.

V. Experiments

The developed dual-arm exoskeleton robot is used to verify the effectiveness of the proposed method, which is shown in Fig. 1, where the Maxon dc flat brushless motor EC45 driven by the servo drive Elmo combined with the harmonic reducer (SHD-20-100-2SH) are used to drive the robot joints, and the force sensors SRI M3203-SN338 (Sunrise Instrument Company, Ltd.) are mounted on the end-effectors of both arms of the exoskeleton robot. The sEMG acquisition device is developed by NCC, Shanghai, China. The sEMG signals of human subject were sampled to calculate the arm endpoint stiffness and the stiffness and position profiles are transferred to the control unit. The control unit uses the stiffness and position profiles to executes the control algorithms to compute the driving torque to the dc motors.

Three healthy human subjects were invited to the experiment. In order to guarantee the objectivity of the experimental results, we specially choose three different conditions of their basic information (subject 1 is fat, 65 kg, 167 cm, 25 years old; subject 2 is normal, 62 kg, 175 cm, 24 years old; subject 3 is thin, 52 kg, 170 cm, 23 years old). Before the experiment, we had given a detailed introduction to all the three subjects about the purpose of the experiment, and make a presentation on experimental steps. During the experiments, the surface electrodes were placed on the surface of the Biceps and Triceps muscle of the left arm of the subject, using the identification results $\bar{K}_J$ and a_{cc}, described in Section III, and combining with human arm Jacobian to calculate the endpoint stiffness in real-time. Table II shows the results of the identified results.

In the manipulation task, the subject held the handle on the end-effector of the left (master) arm of the robotic exoskeleton which used to obtain the interaction force. The left arm of the exoskeleton can be manipulated by the subject to generate the reference trajectories while the subject is allowed to move his arm arbitrarily. Then the position and adaptive stiffness profiles have been transferred from the human (master) arm to the robot (slave) arm, making the robot capable of adapting the stiffness in the interaction tasks.

TABLE II
Results of Identification

	$\bar{K}_J$	r_1	r_2
Subject 1	$\begin{bmatrix}23.54 & 9.61\\ 9.61 & 7.65\end{bmatrix}$	4.058	1.823
Subject 2	$\begin{bmatrix}21.72 & 8.56\\ 8.56 & 6.97\end{bmatrix}$	3.772	1.675
Subject 3	$\begin{bmatrix}20.21 & 7.68\\ 7.68 & 6.39\end{bmatrix}$	3.283	1.482

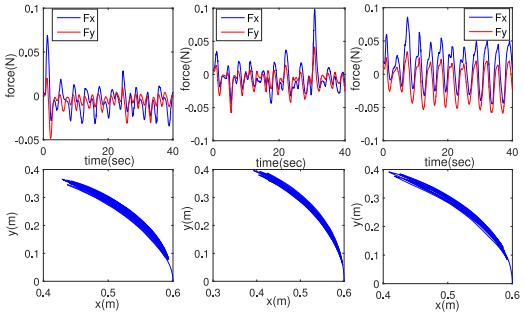

Fig. 2. Typical applied endpoint displacements and restoring forces in x and y directions.

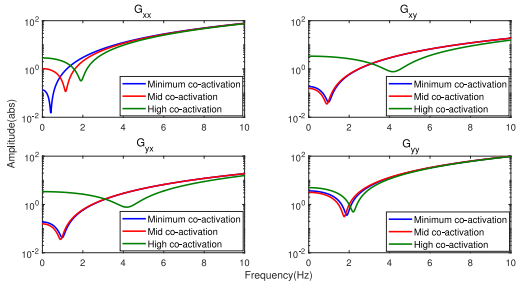

Fig. 3. Human arm endpoint stiffness transfer function estimation obtained from stochastic perturbations.

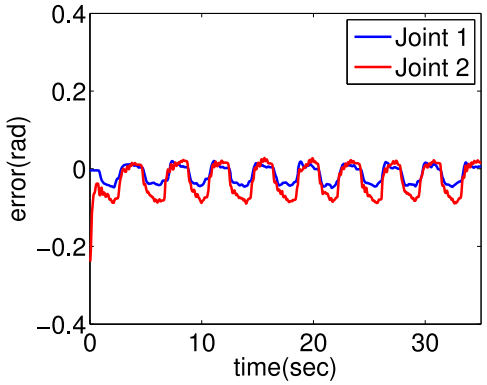

Fig. 4. Tracking error of the subject 1.

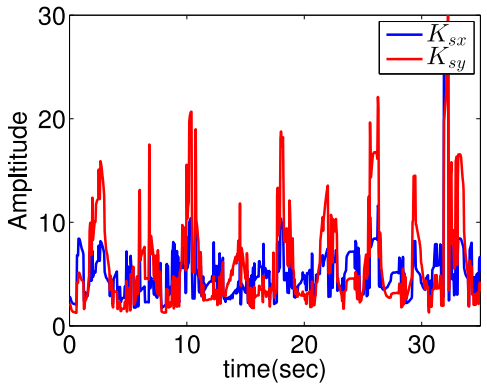

Fig. 5. sEMG calculated stiffness of the subject 1.

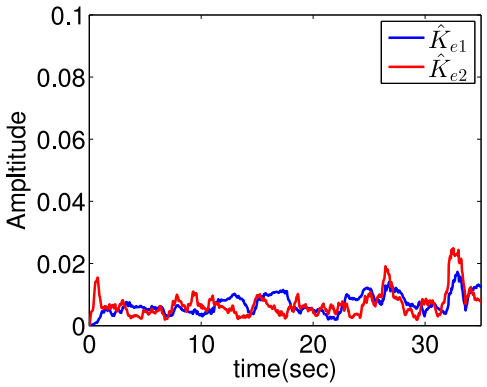

Fig. 6. Adaptive stiffness of the subject 1.

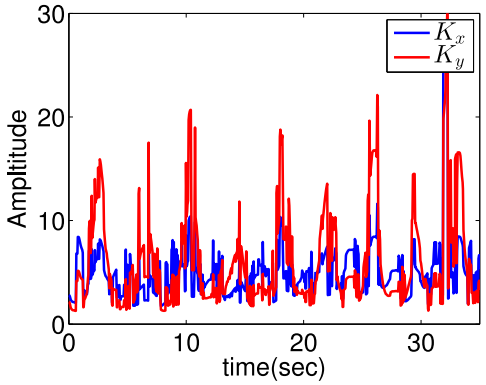

Fig. 7. Final stiffness of the subject 1.

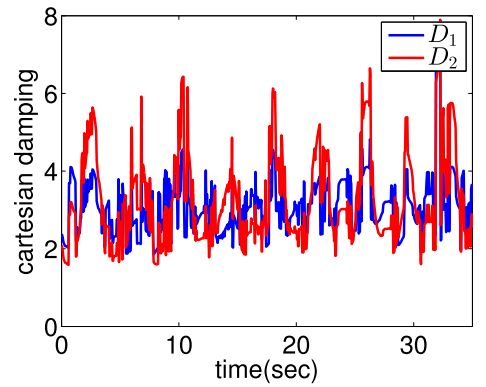

Fig. 8. Damping of the subject 1.

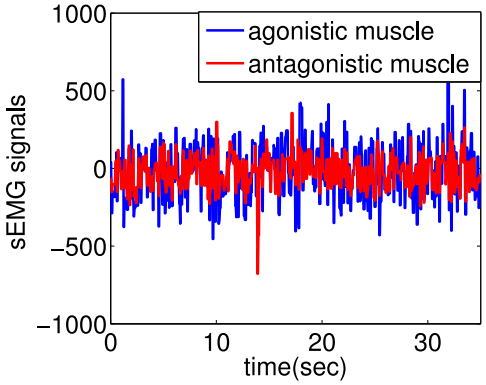

Fig. 9. sEMG signals of the subject 1.

The design parameters used in the experimenter are chosen as $K_m = \text{diag}[3.5, 2.1]$, $\lambda = \text{diag}[5.5, 4.5]$, $\gamma_1 = 0.02$, $\gamma_2 = 0.01$, $\gamma_3 = 0.02$, and $\varsigma_1 = \varsigma_2 = 0.2$. To conclude, the effectiveness of the proposed method can be described as follows.

1) The reference trajectories are transferred to the slave arm according to human arm and tracking errors are bounded based on the proposed controller, which is verified by the experiments in Figs. 4, 12, 13, and 21. Figs. 4 and 13 show the tracking errors of the shoulder joint and the elbow joint. Figs. 4 and 13 show the output of the proposed controller.
2) The impedance parameters can be obtained based on the varying sEMG signals of the human subjects, which has been verified by the experiments in Figs. 5, 7–10, 14, and 16–19. Fig. 6 shows the adaptive stiffness based on the proposed stiffness observer of the subject 1. Those figures show that the impedance parameters changed according to the collected sEMG signals. Fig. 2(a)–(c) illustrates a typical applied endpoint displacements and restoring forces along x, y directions at minimum, mid, and high muscle coactivation level, respectively. Fig. 3 demonstrates the results of second-order model identification of the arm impedance transfer functions in the frequency range from 0 to 10 Hz, according to the identification methods. The stiffness estimation results match similarly with the results in [15].

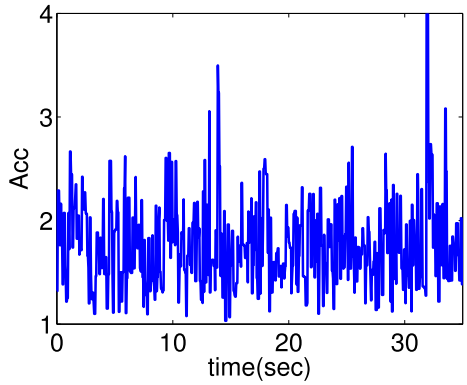

Fig. 10. Co-contraction index Acc of the subject 1.

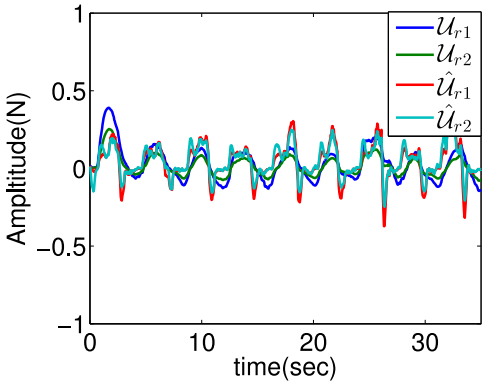

Fig. 11. Interaction force and their estimations of the subject 1.

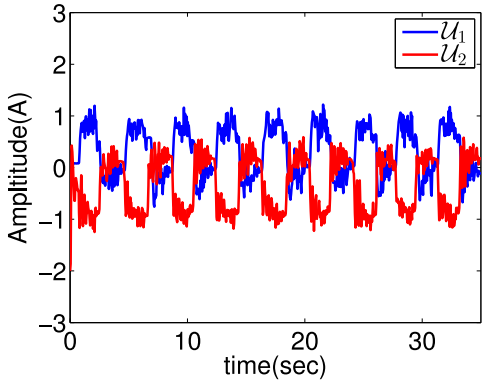

Fig. 12. Driving motor currents of the subject 1.

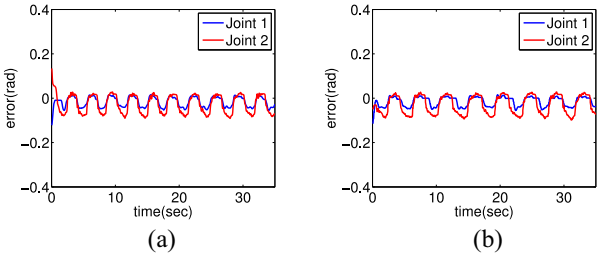

Fig. 13. Tracking error in joint space. (a) Subject 2. (b) Subject 3.

3) The compensated stiffness based on the proposed stiffness observer and the estimated interaction force can be obtained by the experiments in Figs. 5, 11, 15, and 20.

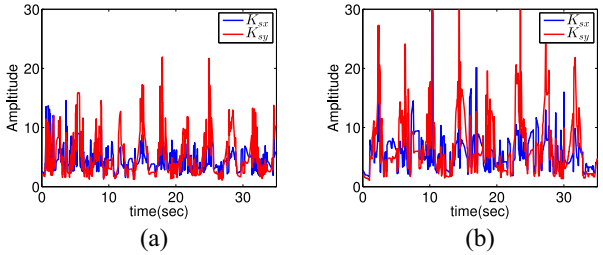

Fig. 14. sEMG calculated stiffness in cartesian space. (a) Subject 2. (b) Subject 3.

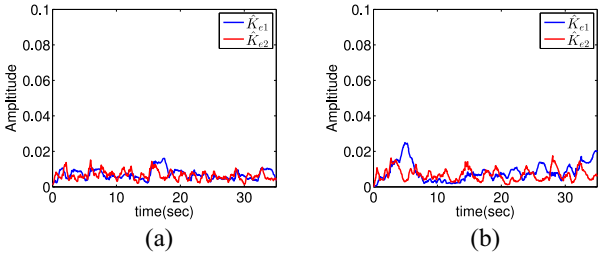

Fig. 15. Adaptive stiffness in cartesian space. (a) Subject 2. (b) Subject 3.

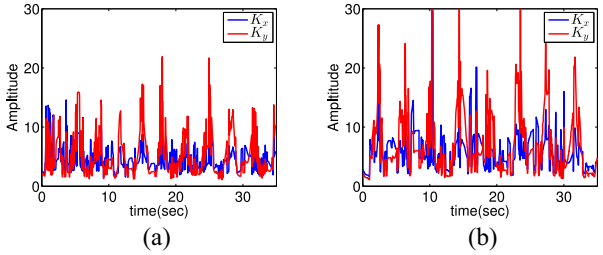

Fig. 16. Final cartesian stiffness. (a) Subject 2. (b) Subject 3.

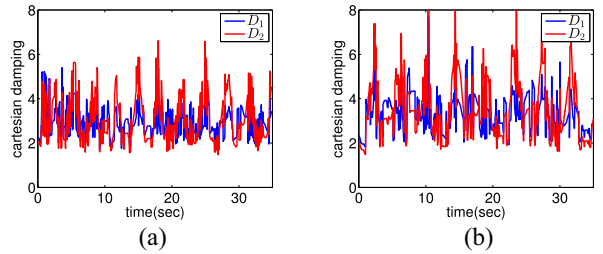

Fig. 17. Cartesian damping. (a) Subject 2. (b) Subject 3.

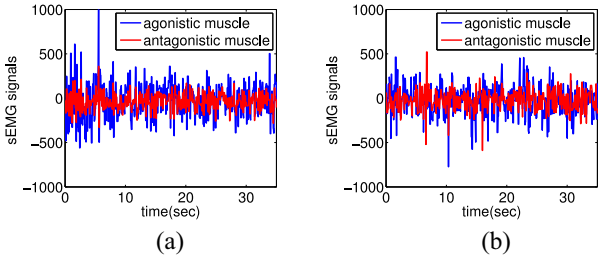

Fig. 18. sEMG signals. (a) Subject 2. (b) Subject 3.

Note that, due to the existence of unknown force, there are errors between the estimated interaction force $\hat{\mathcal{U}}_r$ and the interaction force $\mathcal{U}_r$ measured by the force sensor mounted on

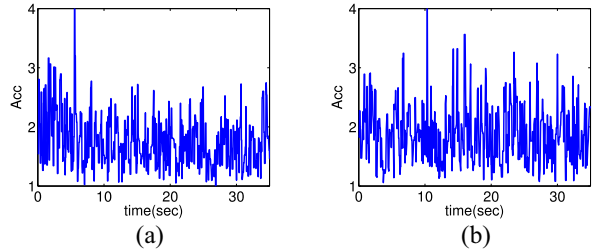

Fig. 19. Co-contraction index Acc. (a) Subject 2. (b) Subject 3.

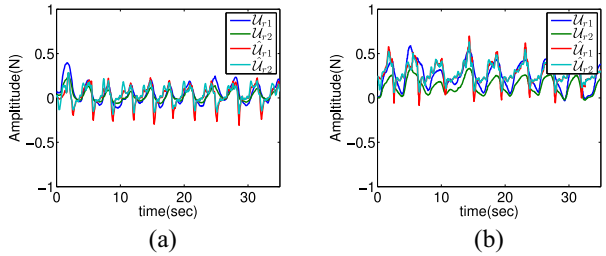

Fig. 20. Interaction force and their estimation in task operation. (a) Subject 2. (b) Subject 3.

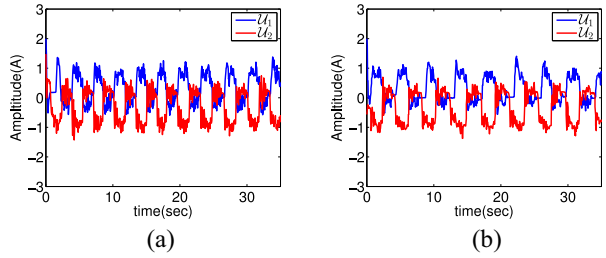

Fig. 21. Driving motor currents. (a) Subject 2. (b) Subject 3.

the effectors. And the errors is compensated by the proposed stiffness observer. We can see that the impedance parameters are adaptive with the sEMG signals synchronously during the movement of the subject's arm. The co-contraction index a_{cc} varies according to the activation of the muscle. Furthermore, Fig. 11 shows the interaction force and their estimation, while Fig. 12 shows the evolution of the input currents for the two joints. From these figures, one can see that the desired performance can be achieved by using the control design presented, even if we do not have the accurate dynamics knowledge of the exoskeleton robot beforehand. Similarly, the experimental results of other two subjects are shown in Figs. 13–21, indicating that the controller is effective among different subjects. To conclude, from these figures, the typical results of the human arm endpoint stiffness tracking utilizing sEMG signals were illustrated, the output of variable stiffness observer to compensate for the errors of calculated stiffness was shown, then the impedance parameters consisted of final Cartesian stiffness and the damping was depicted. The results of the interaction force and their estimations was proven that the impedance and force was adaptive based on designed impedance control. Based on the above obtained parameters and designed controller, the trajectory errors converged, which was less than 0.1 rad, even if we do not have the accurate dynamics knowledge of the exoskeleton robot beforehand. Similarly, the experimental results of other two subjects are shown, indicating that the controller is effective among different subjects to realize skill transfer.

VI. Conclusion

In this paper, force and adaption impedance control of dual-arm exoskeleton manipulation have been presented. We have achieve the utilization sEMG signals to estimate stiffness of human arm and transfer position and stiffness profiles to robot arm in real-time. In addition, in order to further improve the system accuracy, we use a variable stiffness observer to make up for the stiffness estimation errors. Taking the dynamics uncertainties of the exoskeleton robot into consideration, we designed an adaptive robust controller in the task space to compensate for tracking errors. Following the steps to identify human endpoint stiffness, three subject had participated in the experiments to verify the effectiveness of the proposed method. In the future work we will follow on the improvements of control performance and verification of the proposed method on more subjects. Further, we plan to take stroke patients as participants to assist them with rehabilitation training.

References

[1] M. Wilcox, A. Rathore, D. Z. M. Ramirez, R. C. Loureiro, and T. Carlson, "Muscular activity and physical interaction forces during lower limb exoskeleton use," *ASME Trans. Mechatronics*, vol. 3, no. 4, pp. 273–279, 2016.

[2] I. Pedersen and T. Mirrlees, "Exoskeletons, transhumanism, and culture: Performing superhuman feats," *IEEE Technol. Soc. Mag.*, vol. 36, no. 1, pp. 37–45, Mar. 2017.

[3] M. Franken, S. Stramigioli, S. Misra, C. Secchi, and A. Macchelli, "Bilateral telemanipulation with time delays: A two-layer approach combining passivity and transparency," *IEEE Trans. Robot.*, vol. 27, no. 4, pp. 741–756, Aug. 2011.

[4] A. Ajoudani, N. Tsagarakis, and A. Bicchi, "Tele-impedance: Teleoperation with impedance regulation using a body-machine interface," *Int. J. Robot. Res.*, vol. 31, no. 13, pp. 1642–1655, 2012.

[5] N. Karavas *et al.*, "Tele-impedance based assistive control for a compliant knee exoskeleton," *Robot. Auton. Syst.*, vol. 73, pp. 78–90, Nov. 2014.

[6] A. Ajoudani *et al.*, "Exploring teleimpedance and tactile feedback for intuitive control of the Pisa/IIT softhand," *IEEE Trans. Haptics*, vol. 7, no. 2, pp. 203–215, Apr./Jun. 2014.

[7] E. Burdet, R. Osu, D. W. Franklin, T. E. Milner, and M. Kawato, "The central nervous system stabilizes unstable dynamics by learning optimal impedance," *Nature*, vol. 414, no. 6862, pp. 446–449, 2001.

[8] N. Hogan, "Impedance control: An approach to manipulation, part I: Theory; part II: Implementation; part III: Applications," *Trans. ASME J. Dyn. Syst. Meas. Control*, vol. 107, no. 1, pp. 1–24, 1985.

[9] S. Wolf *et al.*, "Variable stiffness actuators: Review on design and components," *IEEE/ASME Trans. Mechatron.*, vol. 21, no. 5, pp. 2418–2430, Oct. 2016.

[10] L. P. J. Selen, P. J. Beek, and J. V. Dieën, "Can co-activation reduce kinematic variability? A simulation study," *Biol. Cybern.*, vol. 93, no. 5, pp. 373–381, 2005.

[11] D. Shin, J. Kim, and Y. Koike, "A myokinetic arm model for estimating joint torque and stiffness from EMG signals during maintained posture," *J. Neurophysiol.*, vol. 101, no. 1, pp. 387–401, 2009.

[12] M. Kawato, "Internal models for motor control and trajectory planning," *Current Opinion Neurobiol.*, vol. 9, no. 6, pp. 718–727, 1999.

[13] M. T. Turvey, "Action and perception at the level of synergies," *Human Movement Sci.*, vol. 26, no. 4, pp. 657–697, 2007.

[14] C. Wang, Y. Li, S. S. Ge, and T. H. Lee, "Reference adaptation for robots in physical interactions with unknown environments," *IEEE Trans. Cybern.*, vol. 47, no. 11, pp. 3504–3515, Nov. 2017.

[15] A. Ajoudani, C. Fang, N. G. Tsagarakis, and A. Bicchi, "A reduced-complexity description of arm endpoint stiffness with applications to teleimpedance control," in *Proc. Int. Conf. Intell. Robots Syst.*, 2015, pp. 1017–1023.

[16] J. Hu, J.-J. Wang, and D. M. Ho, "Design of sensing system and anticipative behavior for human following of mobile robots," *IEEE Trans. Ind. Electron.*, vol. 61, no. 4, pp. 1916–1927, Apr. 2014.

[17] J. K. Salisbury, "Active stiffness control of a manipulator in cartesian coordinates," in *Proc. 19th IEEE Conf. Decis. Control*, 1980, pp. 87–97.

[18] I. Kao and C. Ngo, "Properties of the grasp stiffness matrix and conservative control strategies," *Int. J. Robot. Res.*, vol. 18, no. 2, pp. 159–167, 1999.

[19] D. J. Bennett, "Stretch reflex responses in the human elbow joint during a voluntary movement," *J. Physiol.*, vol. 474, no. 2, pp. 339–351, 1994.

[20] R. Osu and H. Gomi, "Multijoint muscle regulation mechanism examined by measured human arm stiffness and EMG signals," *J. Neurophysiol.*, vol. 81, no. 4, pp. 1458–1468, 1999.

[21] E. J. Perreault, R. F. Kirsch, and P. E. Crago, "Multijoint dynamics and postural stability of the human arm," *Exp. Brain Res.*, vol. 157, no. 4, pp. 507–517, 2004.

[22] H. Gomi and R. Osu, "Task-dependent viscoelasticity of human multijoint arm and its spatial characteristics for interaction with environments," *J. Neurosci.*, vol. 18, no. 21, pp. 8965–8978, 1998.

[23] B. Yuan, M. Sekine, J. Gonzalez, and W. Yu, "Variable impedance control based on impedance estimation model with EMG signals during extension and flexion tasks for a lower limb rehabilitation robotic system," *J. Novel Physiotherapies*, vol. 3, no. 5, pp. 1–10, 2013.

[24] G. Grioli and A. Bicchi, "A non-invasive, real-time method for measuring variable stiffness," in *Proc. Robot. Sci. Syst.*, 2010, pp. 1–5.

[25] H. Kuwahara, T. Shimono, H. Tanaka, D. Yashiro, and K. Ohnishi, "Abstraction of action components unconstrained by alignment of haptic sensing points," *IEEE Trans. Ind. Electron.*, vol. 58, no. 8, pp. 3196–3204, Aug. 2011.

[26] Y. Yang, L. Ma, and D. Huang, "Development and repetitive learning control of lower limb exoskeleton driven by electrohydraulic actuators," *IEEE Trans. Ind. Electron.*, vol. 64, no. 5, pp. 4169–4178, May 2017.

[27] L. Chen, X. Wang, and W. L. Xu, "Inverse transmission model and compensation control of a single-tendon-sheath actuator," *IEEE Trans. Ind. Electron.*, vol. 61, no. 3, pp. 1424–1433, Mar. 2014.

[28] Z. Li, Q. Ge, W. Ye, and P. Yuan, "Dynamic balance optimization and control of quadruped robot systems with flexible joints," *IEEE Trans. Syst., Man, Cybern., Syst.*, vol. 46, no. 10, pp. 1338–1351, Oct. 2016.

[29] Z. Li, C. Yang, and E. Burdet, "Guest editorial An overview of biomedical robotics and bio-mechatronics systems and applications," *IEEE Trans. Syst., Man, Cybern., Syst.*, vol. 46, no. 7, pp. 869–874, Jul. 2016.

[30] Z. Li *et al.*, " Trajectory-tracking control of mobile robot systems incorporating neural-dynamic optimized model predictive approach," *IEEE Trans. Syst., Man, Cybern., Syst.*, vol. 46, no. 6, pp. 740–749, Jun. 2016.

[31] A. Rovetta, R. Sala, X. Wen, and A. Togno, "Remote control in telerobotic surgery," *IEEE Trans. Syst., Man, Cybern. A, Syst., Humans*, vol. 26, no. 4, pp. 438–444, Jul. 1996.

[32] J. Na, Q. Chen, X. Ren, and Y. Guo, "Adaptive prescribed performance motion control of servo mechanisms with friction compensation," *IEEE Trans. Ind. Electron.*, vol. 61, no. 1, pp. 486–494, Jan. 2014.

[33] J. Na, G. Herrmann, X. Ren, M. N. Mahyuddin, and P. Barber, "Robust adaptive finite-time parameter estimation and control of nonlinear systems," in *Proc. IEEE Int. Symp. Intell. Control*, Denver, CO, USA, 2011, pp. 1014–1019.

[34] S. Wang, J. Na, and X. Ren, "RISE-based asymptotic prescribed performance tracking control of nonlinear servo mechanisms," *IEEE Trans. Syst., Man, Cybern., Syst.*, to be published, doi: 10.1109/TSMC.2017.2769683.

[35] Z. Chen, Y.-J. Pan, and J. Gu, "A novel adaptive robust control architecture for bilateral teleoperation systems under time-varying delays," *Int. J. Robust Nonlin. Control*, vol. 25, no. 17, pp. 3349–3366, 2015.

[36] Z. Li, S. S. Ge, M. Adams, and W. S. Wijesoma, "Robust adaptive control of uncertain force/motion constrained nonholonomic mobile manipulators," *Automatica*, vol. 44, no. 3, pp. 776–784, 2008.

[37] C.-T. Chen and W.-D. Chang, "A feedforward neural network with function shape autotuning," *Neural Netw.*, vol. 9, no. 4, pp. 627–641, 1996.

[38] Y. Li and S. S. Ge, "Human–robot collaboration based on motion intention estimation," *IEEE/ASME Trans. Mechatronics*, vol. 19, no. 3, pp. 1007–1014, Jun. 2014.

[39] D. Erickson, M. Weber, and I. Sharf, "Contact stiffness and damping estimation for robotic systems," *Int. J. Robot. Res.*, vol. 22, no. 1, pp. 41–57, 2003.

[40] K. P. Tee, B. Ren, and S. S. Ge, "Control of nonlinear systems with time-varying output constraints," *Automatica*, vol. 47, no. 11, pp. 2511–2516, 2011.

Zhijun Li (M'07–SM'09) received the Ph.D. degree in mechatronics from Shanghai Jiao Tong University, Shanghai, China, in 2002.

From 2003 to 2005, he was a Post-Doctoral Fellow with the Department of Mechanical Engineering and Intelligent systems, University of Electro-Communications, Tokyo, Japan. From 2005 to 2006, he was a Research Fellow with the Department of Electrical and Computer Engineering, National University of Singapore, Singapore, and Nanyang Technological University, Singapore. Since 2012, he has been a Professor with the College of Automation Science and Engineering, South China University of Technology, Guangzhou, China. Since 2017, he has been a Professor with the Department of Automation, University of Science and Technology, Hefei, China. His current research interests include service robotics, tele-operation systems, nonlinear control, and neural network optimization.

Dr. Li has been the Co-Chair of Technical Committee on Bio-mechatronics and Bio-robotics Systems, IEEE Systems, Man, and Cybernetics Society, and Technical Committee on Neuro-Robotics Systems, IEEE Robotics and Automation Society since 2016. He is serving as an Editor-at-Large for the *Journal of Intelligent and Robotic Systems*, and an associate editor of several IEEE TRANSACTIONS. He has been the General Chair and the Program Chair of 2016 and 2017 IEEE Conference on Advanced Robotics and Mechatronics, respectively.

Cuichao Xu received the B.S. degree in vehicle engineering from the Hefei University of Technology, Hefei, China, in 2017. She is currently pursuing the M.S. degree in control theory and control engineering with the University of Science and Technology of China, Hefei.

Her current research interest includes mechanical design, simulation, and control.

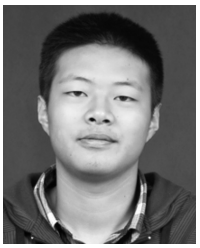

Qiang Wei received the B.S. degree in automation from the University of Electronic Science and Technology of China, Chengdu, China, in 2015. He is currently pursuing the Ph.D. degree in control theory and control engineering with the University of Science and Technology of China, Hefei, China.

His current research interests include exoskeleton robotics, synergy-based control, and biosignal processing.

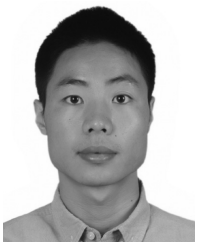

Chao Shi received the M.S. degree from the College of Automation Science and Engineering, South China University of Technology, Guangzhou, China, in 2018.

He is currently with China Merchants Bank Network Technology in Shenzhen, Guangdong, China. His current research interests include robotics, intelligent control, and human–robot interaction.

Chun-Yi Su (SM'99) received the Ph.D. degree in control engineering from the South China University of Technology, Guangzhou, China, in 1990.

After a seven-year stint with the University of Victoria, Victoria, BC, Canada, he joined Concordia University, Montreal, QC, Canada, in 1998. He conducts research in the application of automatic control theory to mechanical systems. He is particularly interested in control of systems involving hysteresis nonlinearities. He has authored or coauthored over 300 publications, which have appeared in journals, as book chapters, and in conference proceedings.

Dr. Su has served as an Associate Editor for the IEEE TRANSACTIONS ON AUTOMATIC CONTROL and IEEE TRANSACTIONS ON CONTROL SYSTEMS TECHNOLOGY, and *Journal of Control Theory and Applications*. He is on the editorial board of 14 journals, including IFAC journals of *Control Engineering Practice* and *Mechatronics*. He has also severed for many conferences as an organizing committee member, including the General Co-Chair of the 2012 IEEE International Conference on Mechatronics and Automation, and the Program Chair of the 2007 IEEE Conference on Control Applications.